Research Article GU J Sci 35(2): 404-419 (2022) DOI: 10.35378/gujs.838992

Gazi University

Journal of Science

http://dergipark.gov.tr/gujs

# Spectroscopic and Quantum Chemical Studies on the Structure of 3-chloro-2-{(2Z)-2-[1-(4-methoxyphenyl)ethylidene]hydrazinyl}pyridine

Tufan TOPAL*

*Pamukkale University, Department of Chemistry, 20020, Denizli, Turkey*

## Highlights

- Synthesis of the new pyridine-hydrazone compound.
- Spectroscopic and structural characterization.
- Quantum calculations related to the HL molecule.

**Article Info**

*Received: 10 Dec 2020*
*Accepted: 09 May 2021*

**Keywords**

*DFT calculations*
*Gaussian 09W*
*FT-Raman*
*Hydrazone*
*Pyridine*

## Abstract

3-chloro-2-{(2Z)-2-[1-(4-methoxyphenyl)ethylidene]hydrazinyl}pyridine (HL) was prepared and its structure elucidated by LC/MS-MS, $^{1}$H and $^{13}$C-NMR, UV-Vis, elemental analysis, FT-Raman and FT-IR. All theoretical calculations and optimized geometry were obtained from the 6-31G(d,p) basis set calculations. Calculated and scaled data of the molecule were compared with the observed FT-Raman and FT-IR spectroscopic data. The theoretical chemical shifts of the HL were performed in chloroform by using the same level with the GIAO method. The UV-Vis analyses of the HL were carried out at three different concentrations in chloroform and ethanol solvents and between 240-440 nm; the calculations of UV-Vis spectra analyses were performed via the TD-DFT method. The charge transfer and hyperconjugative and conjugative interactions were analyzed using the NBO analysis. Furthermore, frontier molecular orbitals (FMOs) and molecular electrostatic potential (MEP) were also measured using the same method. This work provides a comprehensive electronic properties, vibration analysis and structural information of the title compund.

## 1. INTRODUCTION

Hydrazone and its derivatives are frequently studied compounds due to their biological behaviour as anti-cancer, antifungal and antibacterial [1]. They also display optoelectric properties, luminescence, supramolecular order, magnetism and redox activities [2]. Hydrazones are often utilised because of their ability to coordinate with metals, especially lanthanide ion forms, to create multicoloured complexes that have recently been used to identify ions inside cancer cells [3]. Some hydrazone substances have also been used in synthetic, industrial, coordination chemistry and medical. In the hydrazone moiety involving azomethine group atoms, the carbon atoms are of an electrophilic and nucleophilic character, while nitrogen atoms are of nucleophilic character. With that unique dynamic, hydrazones play an important role in studies to develop new drugs [4, 5]. Meanwhile, pyridines containing heterosubstitutes are biologically active compounds, and compounds involving the pyridine rings play a similarly significant role in various living systems, including ones involving antibiotics, coenzymes, vitamins and nucleic acids [6]. Beyond that, derivatives of pyridine compounds are used as drugs for brain diseases, anaesthetic agents, agricultural products and pharmaceutical drugs [7]. Because the molecule that we studied is based on both hydrazone and pyridine, it is thought to have exceptionally high biological activity. Theoretical studies of compounds provide important information about their physical and chemical properties. To date, extensive theoretical work has been conducted to validate, understand and interpret experimental studies based on quantum mechanics, especially concerning pharmacology, the synthesis of new disease-fighting drugs and the estimation of the binding mechanisms of small molecules on target biological proteins. As a result, theoretical studies have saved time and reduced costs [8]. Density functional theory (DFT), widely applied theoretical method, ranks amongst the most important tools used for predicting structures in computational

*e mail: tufantopal@hotmail.com

chemistry. The presence of functional groups in chemical molecules and the intensities of different peaks can be determined by FT-IR/FT-Raman spectra, supported by scaling factors applied to eliminate systematic errors and ensure theoretical and experimental compatibility [9]. In interpreting the experimental spectra of molecules, the wavelengths estimated by DFT, spectral intensities and potential energy distribution (PED) make a valuable contribution [10,11].

In this study, HL molecule consisting of pyridine and hydrazone moieties was characterized with spectroscopic methods and theoretical calculations were made to determine the dynamic behaviour of the structure. Systematic assays were performed on the optimised structure, including vibrational spectra, NMR, natural bonding orbitals (NBO), UV-Vis, highest occupied molecular orbitals (HOMO), lowest unoccupied molecular orbitals (LUMO) and MEP analyses. With those theoretical calculations, the charge transfer from donors to acceptors, electronic transition, chemical reactivity descriptors (e.g. softness and hardness), electronegativity and electrostatic potential values were examined. The data recorded from the experiment were compared with the calculated data, for results discussed later in this report.

## 2. MATERIAL AND METHOD

### 2.1. Materials and Physical Measurements

A Bruker BioSpin NMR Avance Spectrometer-III (400 MHz) was used for NMR analysis, with elemental analysis rates of the molecule determined by a Thermo Finnigan FlashEA 1112 analyser. IR analysis was performed using a Perkin Elmer FTIR-Spectrometer device between 400–4000 $cm^{-1}$, and the mass spectrometry analysis was determined with a TSQ Fortis™ Triple Quadrupole Mass Spectrometer device. Raman analysis was performed using a Thermo Fisher Scientific DXR™ 3xi Raman imaging microscope equipped with an Nd: YAG laser source operating at 1064-nm line widths between 10–4000 $cm^{-1}$. The melting point was determined with a Stuart SMP10 apparatus. Absorption spectra were determined with a Shimadzu UV-1800 spectrophotometer. Ethanol, acetonitrile, 3-chloro-2-hydrazinopyridine and 4'-methoxyacetophenone were purchased from Sigma–Aldrich.

### 2.2. Synthesis of HL

The preparation of the ligand (i.e. HL) has been described previously [12]. For the solution, 0.1435 g (1 mmol) of 3-chloro-2-hydrazinopyridine in 10 $cm^3$ of acetonitrile was mixed with 0.1501 g (1 mmol) of 4'-methoxyacetophenone in 15 $cm^3$ of acetonitrile. The solution was stirred for 24 h at 20 °C and then filtered. The solid product obtained was washed several times with ultrapure water, recrystallised from hot acetonitrile and dried over anhydrous $P_2O_5$.

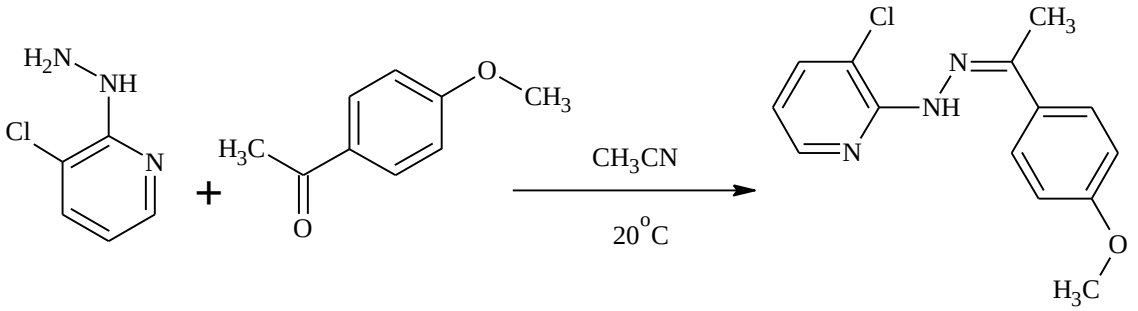


***Figure 1.*** *Reaction scheme of the HL molecule*

$C_{14}H_{14}ClN_3O$ [HL], Crem; Yield 78%. M.p.: 119-121 °C. $^1$H-NMR (400 MHz, Chloroform-$d_6$, ppm): δ 8.28 (s, 1H, -NH), δ 8.24 (1H, Ar-H), δ 7.82 (2H, Ar-H), δ 7.57 (1H, Ar-H), δ 6.92 (2H, Ar-H), δ 6.76 (1H, Ar-H), δ 3.83 (3H, O-$CH_3$), δ 2.33 (3H, -$CH_3$), $^{13}$C-NMR (100 MHz, Chloroform-$d_6$, ppm): δ 150.65 (C-Ar), δ 147.85, δ 147.08 (C-$Ar_{pyridine}$), δ 136.88 (-C=N-), δ 131.15 (C-Ar), δ 128.28 (C-$Ar_{pyridine}$), δ 127.78, 127.78 (C-Ar), δ 115.65, δ 114.97 (C-$Ar_{pyridine}$), δ 113.69, δ 113.69 (C-Ar), δ 55.31 (O-$CH_3$), δ 12.85 (-$CH_3$). LC/MS-MS Ms: (ESI) m/z= 275.73 $[M+1]^+$ (100). Calcd. for [HL]: C, 60.98; H, 5.12; N, 15.24%; Found:

C, 60.95; H, 5.17; N, 15.20%. FT-IR ($cm^{-1}$): 3340 (N-H), 3015 (C-$H_{Ar}$), 1608 (C=N), 424 (C-Cl). FT-Raman ($cm^{-1}$): 3351 (N-H), 3010 (C-$H_{Ar}$), 1600 (C=N), 421 (C-Cl). The reaction scheme (Figure 1) and optimized structure of the HL compound with atom labels are presented in Figure 2.

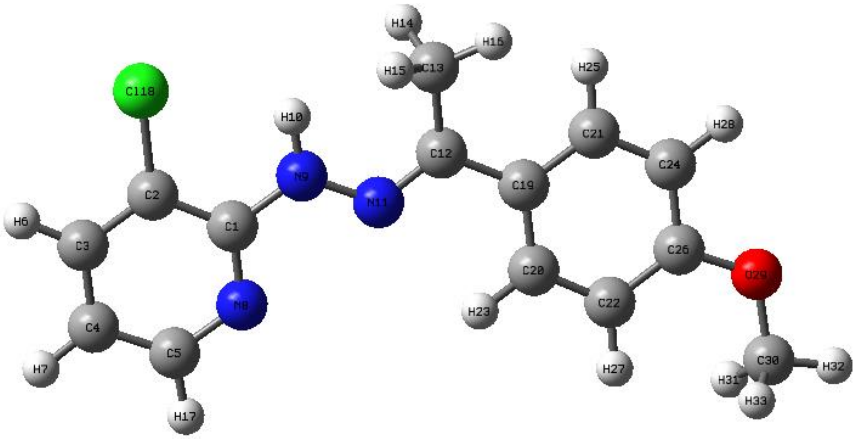


***Figure 2.*** *Optimized geometric structure of HL molecule*

### 2.3. Computational Details

The geometry of the HL was optimised following the DFT/B3LYP(Becke3–Lee–Yang–Parr)/6-31G(d,p) method [13–15]. The minimum energy configuration of surface potential energy achieved by optimising the molecule and the stability of the optimised geometries were confirmed by calculating wavenumbers. The same basis set was used to determine vibrational wavenumbers by using the optimised structure. The scaling factor (http://cccbdb.nist.gov/vsfx.asp) of 0.961 was applied to the computed wavenumbers, often used to accurately predict the vibration spectra of molecules, makes theoretical and experimental calculations more compatible with each other [9,16]. The PED was computed by using the program VEDA 4, which was also used to detail the vibrational modes obtained in experiment [17]. The theoretical NMR data were computed in chloroform using the gauge including atomic orbitals (GIAO) approach at the GIAO-DFT/B3LYP/6-31G(d,p) [18], while UV spectra energies were computed with TD–DFT method [19]. The NBO properties, HOMO-LUMO and MEP were achieved using the same level [20]. The ground state equilibrium structure of the HL molecule, the Gaussian 09W package and the Gauss-view 6.0 visualisation program were used for all theoretical calculations [21,22], along with GAMESS (US) [23].

## 3. RESULT AND DISCUSSION

### 3.1. Vibrational Spectra Analysis

Once the pyridine-derived material was synthesised, the characterisation of the structure was verified by comparison with the literature. According to our results, the HL molecule had a C1 symmetry group and 93 vibrational fundamental normal modes and consisted of pyridine (Arpyridine-N) and 4-methoxyphenyl rings, a hydrazone group (-NHN=CH-) and methyl (-$CH_3$) and methoxy (O–$CH_3$) groups. The spectral assignments of the scaled FT-IR wavenumbers selected calculated and basic vibration modes with the calculated FT-IR intensities and observed FT-IR/FT-Raman bands are given in Table 1. Negative values in PED analyses indicate asymmetrical stretching vibrations, whereas positive ones indicate symmetrical vibrations.

***Table 1.*** *Selected vibrational assignments of the HL molecule*

| Calculated | | Observed | | |
|---|---|---|---|---|
| DFT/B3LYP | IR Intensity (km/mole) | IR | Raman | Assignments(%PED)≥10% |
| 3435 | 19,05 | 3340 | 3351 | ν NH(100) |

| | | | | |
|---|---|---|---|---|
| 3084 | 4,97 | 3085 | 3083 | ν CH(97) |
| 3072 | 12,12 | | 3063 | ν CH(-93) |
| 3026 | 30,15 | 3015 | 3010 | ν CH(91) |
| 2959 | 43,16 | 2967 | | ν CH(-100) |
| 2959 | 12,00 | | 2921 | ν CH(99) |
| 2910 | 11,78 | | 2915 | ν CH(93) |
| 2899 | 64,67 | 2840 | | ν CH(91) |
| 1609 | 152,32 | 1608 | 1600 | ν NC(-60)+ δ HCC(12) |
| 1588 | 34,53 | 1584 | 1570 | ν NC(-49) |
| 1580 | 476,11 | | | ν CC(26)+ ν CC(-13) |
| 1555 | 9,00 | | 1558 | ν CC(36) |
| 1549 | 1,87 | | | ν CC(28)+ ν CC(-16) |
| 1509 | 72,51 | | 1513 | ν CC(-16)+ δ HNN(14)+ δ HCC(-12) |
| 1494 | 353,25 | 1492 | | δ HNN(13)+ δ HCC(32) |
| 1438 | 147,02 | 1448 | | ν CC(23)+ δ HCN(22)+ δ HCH(-23) |
| 1431 | 28,61 | 1417 | 1414 | δ HCH(79) |
| 1403 | 2,46 | | | ν CC(-37)+ δ HCC(-32) |
| 1386 | 122,89 | 1394 | | ν NC(12)+ δ HNN(18)+ δ HCC(24) |
| 1360 | 15,10 | 1339 | 1340 | δ HCH(85) |
| 1265 | 9,99 | 1245 | 1256 | ν NC(71) |
| 1251 | 372,11 | 1233 | 1246 | ν OC(55)+ δ HCC(-10) |
| 1215 | 93,96 | | 1234 | ν CC(-13)+ δ HCC(25)+ δ HCN(10) |
| 1164 | 8,32 | 1189 | 1178 | δ HCH(-19)+ τ HCOC(-62) |
| 1160 | 66,52 | 1179 | | ν NC(11)+ δ HCC(-67) |
| 1106 | 21,61 | 1106 | 1108 | ν CC(13) + δ HCC(30)+ δ HCC(-21) |
| 1097 | 52,26 | | 1078 | ν CC(-10)+ ν NN(-15)+ δ HCC(15)+ δ HCC(22) |
| 1060 | 0,29 | | 1061 | ν CC(-13)+ δ HCC(-10)+ τ HCCC(15) |
| 1048 | 8,85 | | | ν CC(33)+ δ HCC(13) |
| 1030 | 61,85 | 1026 | 1024 | ν OC(74) |
| 993 | 63,92 | | | ν ClC(-12)+ δ CCC(-40) |
| 985 | 0,29 | | | δ HCC(-18)+ δ CCC(66) |
| 946 | 19,14 | 965 | | ν CC(-28)+ τ HCCC(-17) |
| 935 | 0,69 | 931 | | τ HCCC(78)+ τ HCCC(-10) |
| 914 | 0,41 | | 908 | τ HCCC(-74) |
| 886 | 0,30 | 830 | | ν CC(-12)+ ν CC(10)+ ν NC(17) |
| 814 | 48,70 | 810 | 807 | τ HCCC(61)+ γ CCNC(12) |
| 761 | 23,17 | 756 | 771 | τ HCCC(15)+ τ HCCC(70) |
| 736 | 47,45 | 742 | | ν ClC(15)+ δ CCC(-13) |
| 723 | 16,46 | | | τ CCCC(-10)+ τ CNCC(-64) |
| 704 | 0,55 | | | τ CCCC(-65) |
| 627 | 2,40 | | | ν CC(15)+ δ CCC(69) |
| 536 | 5,18 | | | τ CCCC(-54) |
| 433 | 4,35 | 443 | | τ HCCC(-10)+ γ ClCCC(-70) |
| 420 | 16,77 | 424 | 421 | ν ClC(-14)+ δ CCN(36) |
| 407 | 0,58 | | | τ CCCC(71) |

| | | | | |
|---|---|---|---|---|
| 293 | 4,05 | | | δ CCC(61) |
| 275 | 0,23 | | | γ ClCCC(26)+ τ CCNN(24) |

δ: in-plane-bending, γ: out-of-plane bending, ν: stretching, τ: torsion, Potential Energy Distribution (%PED)

Of all basic vibration modes torsion, in-plane and out-of-plane bending and stretching in organic compounds, N–H stretching vibration bands are generally found at 3000–3500 $cm^{-1}$ [24]. That band, calculated as 3435 $cm^{-1}$ in the HL compound, was recorded at 3340/3351 $cm^{-1}$ in FT-IR/FT-Raman spectra. PED analysis showed that the mode was 100% stretching vibration. Characteristic C–H stretching vibration bands, by contrast, are generally found at 3000–3100 $cm^{-1}$ [25]. In pyridine and 4-methoxyphenyl rings, the peaks observed at 3015 and 3085 $cm^{-1}$ in FT-IR, at 3010, 3063 and 3083 $cm^{-1}$ in FT-Raman can be attributed to the C–H peaks. The C–H peak values were calculated between 3026–3084 $cm^{-1}$, and PED analyses of C–H stretching vibrations were found at a rate of 91-99%. In past research, the C–H band has been observed at 800–950/1000–1300 $cm^{-1}$ [26]. The peaks computed at 985, 1048-1160, 1215 and 1251 $cm^{-1}$ were assigned C–H in-plane bending vibrations, and those vibrations were observed in the HL molecule at 1026, 1179 and 1233 $cm^{-1}$ in FT-IR, at 1078, 1178 and 1246 $cm^{-1}$ in FT-Raman spectrum. C–H torsion vibrations in the pyridine and 4-methoxyphenyl rings were calculated in the range of 761–814 and 914–946 $cm^{-1}$ in simulated calculations and observed at 756/771 $cm^{-1}$ in FT-IR/FT-Raman spectra. The experimental FT-IR/FT-Raman spectra, along with the FT-IR spectrum calculated with the scaling factor, appear in Figures 3a and 3b [27].

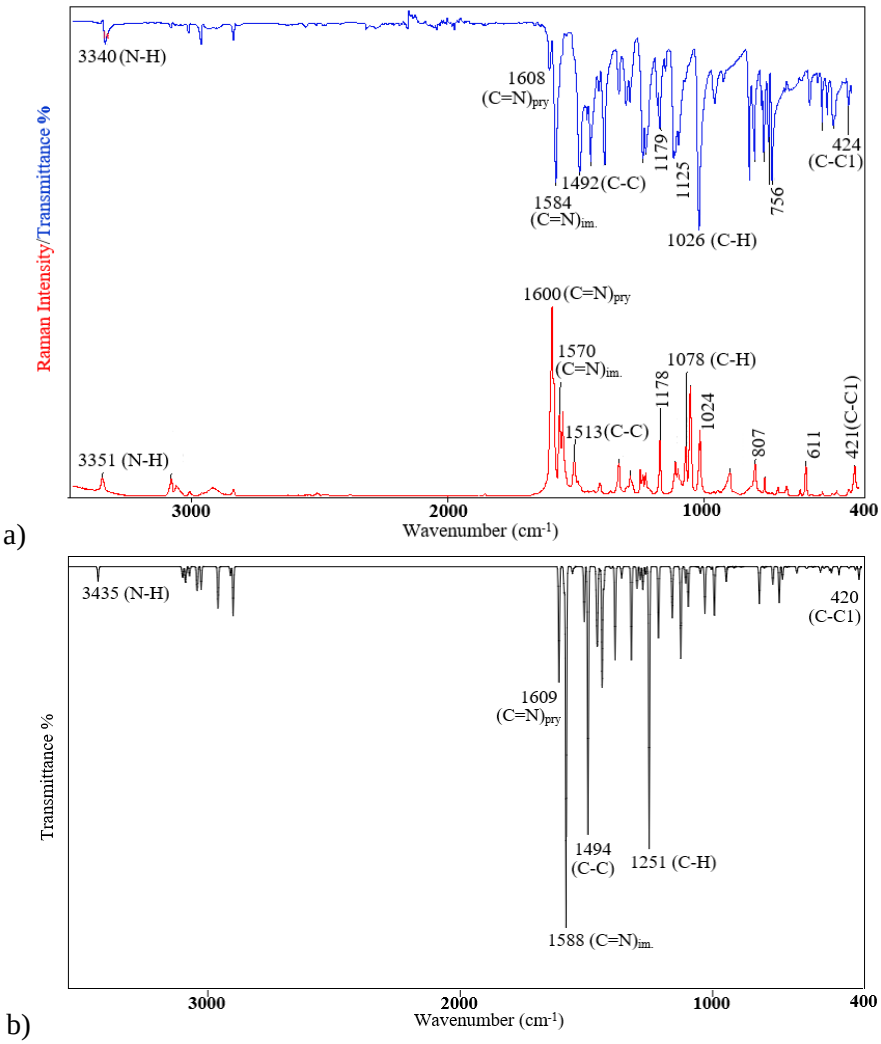


***Figure 3.*** *a) The experimental FT-IR (top) and FT-Raman (bottom) b) the calculated FT-IR (scaled) spectra of the HL molecule*

In general, stretching vibration bands in the range 1400–1650 $cm^{-1}$ in pyridine compounds are attributed to C–C bands [28]. The computed values at 1403, 1438, 1509-1580 $cm^{-1}$ indicate good agreement with the experimental bands recorded at 1492/1513 $cm^{-1}$ in FT-IR/FT-Raman spectra. According to the B3LYP method, the vibration bands observed at 293, 627, 736, 985 and 993 $cm^{-1}$ represent C–C–C in-plane bending vibrations modes in the ring, whereas the torsion bands at 407, 536, 704 and 723 $cm^{-1}$ indicate the C–C–C–C mode [29]. While C–H stretching vibrations in the methyl group were observed at 2910/2959 $cm^{-1}$, vibrations in the methoxy group were observed at 2899/2910 $cm^{-1}$. Those results are largely consistent with published data [30]. Beyond that, the asymmetrical vibration mode of the methylene group was observed at 2967 $cm^{-1}$ in FT-IR, while the symmetric vibration mode of the methoxy group was recorded at 2840 $cm^{-1}$. The FT-IR band at 1339, 1417 and 1448 $cm^{-1}$ and the FT-Raman band at 1340 and 1414 $cm^{-1}$ can be attributed to $CH_3$ vibration and simulated values in the range of 1360–1438 $cm^{-1}$. Methoxy groups generally give asymmetrical vibration bands between 1210 and 1310 $cm^{-1}$ and symmetrical vibration bands between 1010 and 1050 $cm^{-1}$ [31]. The vibration of that group was observed at 1026 and 1189 $cm^{-1}$ in FT-IR and at 1024 and 1178 $cm^{-1}$ in FT-Raman, and bands at 1030, 1164 and 1251 $cm^{-1}$ were calculated for the HL molecule [32]. The C=N vibration was assigned to the bands at 1584 and 1608 $cm^{-1}$ in FT-IR and at 1570 and 1600 $cm^{-1}$ in FT-Raman. By extension, values of C=N vibration were calculated at 1588 and 1609 $cm^{-1}$ for the hydrazone moiety and pyridine ring of the imine group [9]. Estimated values of the C–Cl vibration band calculated at low wavelengths were found at 275, 420 and 433 $cm^{-1}$ with PED (≥10%), and the C–Cl band was observed at 424 $cm^{-1}$ in the FT-IR and at 421 $cm^{-1}$ in the FT-Raman [33]. The correlation graph of the HL molecule with the vibration frequencies was calculated (scaled) following the DFT/B3LYP method, and the observed data are given in Figure 4. The graph shows the linear correlation between experimental and theoretical frequencies, such that the equation y = 0.9881x + 8.5079 ($R^2$ = *0.9993*) could be obtained. According to the results, the experimental and theoretical data agree clearly.

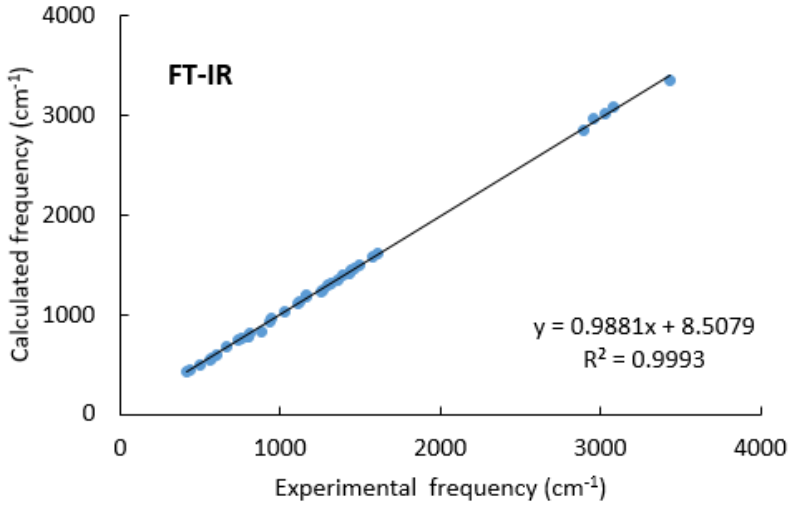


***Figure 4.*** *The correlation graph between the experimental and calculated frequencies of the HL molecule*

### 3.2. NMR Analysis

Using NMR and quantum chemistry calculation methods in combination is an effective way to interpret the structure of molecules. Theoretical chemical shift values of HL were estimated using the TMS shielding calculation and the TMS B3LYP/6-311+G(2d,p) GIAO level as a reference [32]. The $^1$H-NMR spectrum of the HL molecule (N–H) proton (H10) was recorded at 8.28 ppm as a singlet peak. In the pyridine and 4-methoxyphenyl rings, protons were observed at 6.76, 6.92, 6.92, 7.57, 7.82, 7.82 and 8.24 ppm (H7, H28, H27, H6, H25, H23 and H17 atoms, respectively) in the $^1$H-NMR spectrum. The signals at 6.92 and 7.82 ppm, the peak areas of which corresponded to the two protons, were attributed to (H28 and H27) and (H25 and H23) atoms, respectively. The spectrum of the HL molecule was observed as singlet peaks at 2.33 ppm in methylene (H14, H15 and H16) and 3.83 ppm in methoxy (H31, H32 and H33) groups of protons. The computed values of the $^1$H-NMR chemical shift of the methoxy and methylene groups were at 3.85, 4.13 and 3.85 ppm and 1.95, 2.08 and 2.57 ppm, respectively [34]. $^1$H and $^{13}$C-NMR spectra of HL are given in

Figures 5a and 5b. The resonance at the 160.30 ppm (i.e. for C26) in the decoupled $^{13}$C-NMR spectrum of the ligand was greater than in the other aromatic groups of carbons. The experimental shift values of the pyridine and 4-methoxyphenyl rings of carbons were observed in the range of 113.69–160.30 ppm, whereas those carbons computed from DFT were in the range of 96.47–144.30 ppm. The imine carbon peak (C12) of the hydrazone group (-NHN=CH) was determined at 147.08 ppm, while the resonance of that group of (C=N) carbon were predicted at 130.14 ppm [35]. The calculated and recorded NMR values of protons and carbons are tabulated in Table 2.

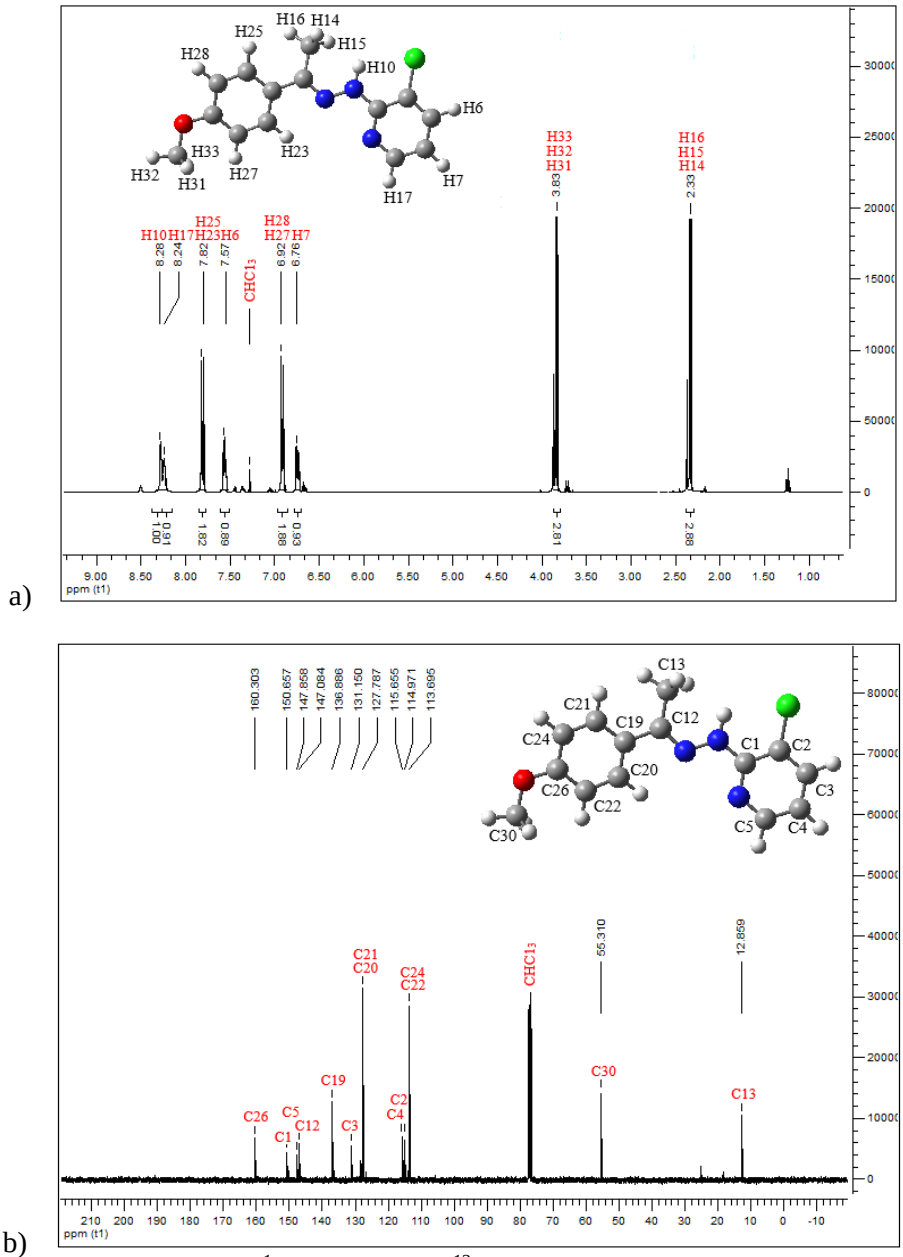


***Figure 5.*** *a) $^{1}$H-NMR and b) $^{13}$C-NMR spectrum of HL*

The peaks at 12.85 and 55.31 ppm, respectively attributed to the methylene and methoxy groups of carbon (C13) and (C30), were calculated as 1.50 and 43.34 ppm, also respectively. The (C30) carbon of the O–$CH_3$ group demonstrated a higher chemical shift at $^{13}$C NMR than the $CH_3$ group of the (C13) carbon [30]. The correlation equalities for $^{1}$H and $^{13}$C -NMR by using the same method were y = 0.9454x + 0.2221 ($R^2$= *0.9866*) and y= 1.029x + 10.721 ($R^2$ = *0.9917*), respectively (Figure 6). Those values are highly compatible with the recorded values and estimated chemical shift values obtained.

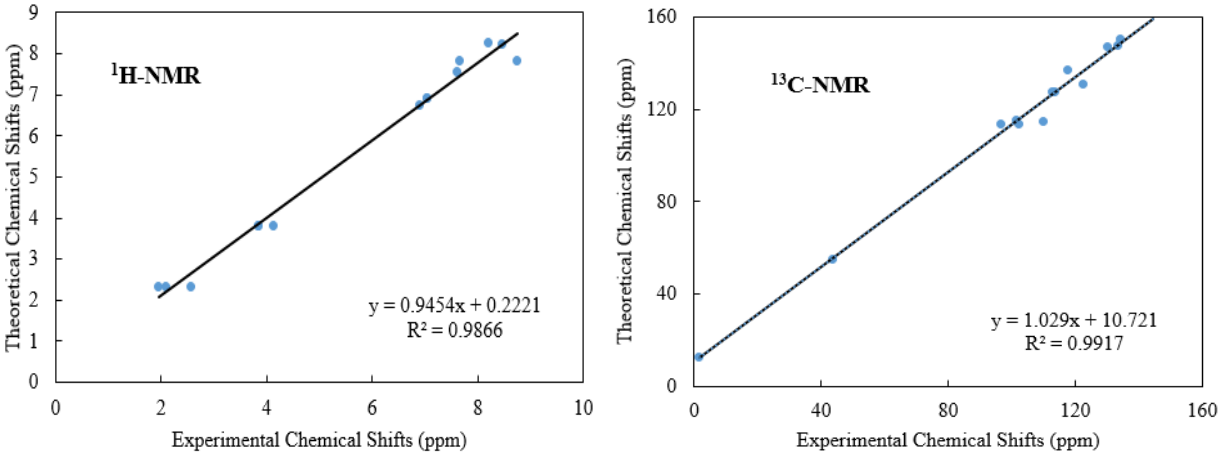


***Figure 6.*** *The correlation graphic of theoretical and experimental NMR of the HL molecule*

***Table 2.*** *Chemical shifts of the HL molecule*

| Atom | Experimental | DFT | Atom | Experimental | DFT |
|---|---|---|---|---|---|
| H(10) | 8.28 | 8.20 | C(26) | 160.30 | 144.30 |
| H(17) | 8.24 | 8.46 | C(1) | 150.65 | 134.33 |
| H(23) | 7.82 | 8.75 | C(5) | 147.85 | 133.39 |
| H(25) | 7.82 | 7.65 | C(12) | 147.08 | 130.14 |
| H(6) | 7.57 | 7.60 | C(19) | 136.88 | 117.50 |
| H(27) | 6.92 | 7.04 | C(3) | 131.15 | 122.40 |
| H(28) | 6.92 | 7.04 | C(20) | 127.78 | 113.49 |
| H(7) | 6.76 | 6.90 | C(21) | 127.78 | 112.52 |
| H(31) | 3.83 | 3.85 | C(4) | 115.65 | 101.43 |
| H(32) | 3.83 | 4.13 | C(2) | 114.97 | 109.99 |
| H(33) | 3.83 | 3.85 | C(22) | 113.69 | 96.47 |
| H(14) | 2.33 | 1.95 | C(24) | 113.69 | 102.28 |
| H(15) | 2.33 | 2.08 | C(30) | 55.31 | 43.34 |
| H(16) | 2.33 | 2.57 | C(13) | 12.85 | 1.50 |

### 3.3. Ultraviolet (UV) and Electronic Properties Analysis

The UV-Vis analyses of the HL molecule were carried out at three different concentrations ($5\times10^{-5}$, $10\times10^{-5}$ and $15\times10^{-5}$ mol $L^{-1}$) in ethanol and chloroform solvents and between 240-440 nm wavelength region. The calculations of UV-Vis spectra analyses were conducted by (Time-dependent) TD-DFT method with 6-31G(d,p) level (ethanol and chloroform as solvents) using Gaussian 09W program [19]. That program gives us information about the HL molecule excitation energies, wavelengths and oscillator strengths [7,30]. Absorption spectra of HL in chloroform and ethanol solvents are given in Figure 7a. The absorption spectra in ethanol shown in Figure 7b were recorded for three different concentrations [36]. The theoretical UV-Vis spectrum of HL in ethanol and chloroform solvents shown in Figures 7c and 7d. It was observed that the maximum absorbance peaks of the HL molecule prepared in different concentrations in ethanol and chloroform solvents were in harmony with each other (Table 3). The TD-DFT calculations of predicted electronic transitions at 335/336 nm with oscillator strengths 0.77/0.78 corresponding to ethanol/chloroform are in excellent agreement with the recorded spectra ($\lambda_{exp.}$= 331/333 nm in ethanol and chloroform respectively) [30]. As shown in Table 3, two strong bands (331/333 and 291/293 nm), observed in ethanol and chloroform solutions, are assigned to n-π * and π-π * transitions, respectively [37]. While the n-π* transitions of the compounds originated from the hydrazone group (-NHN=CH) of atoms, the π-π* band occurred due to the electrons of the pyridine ring [38].

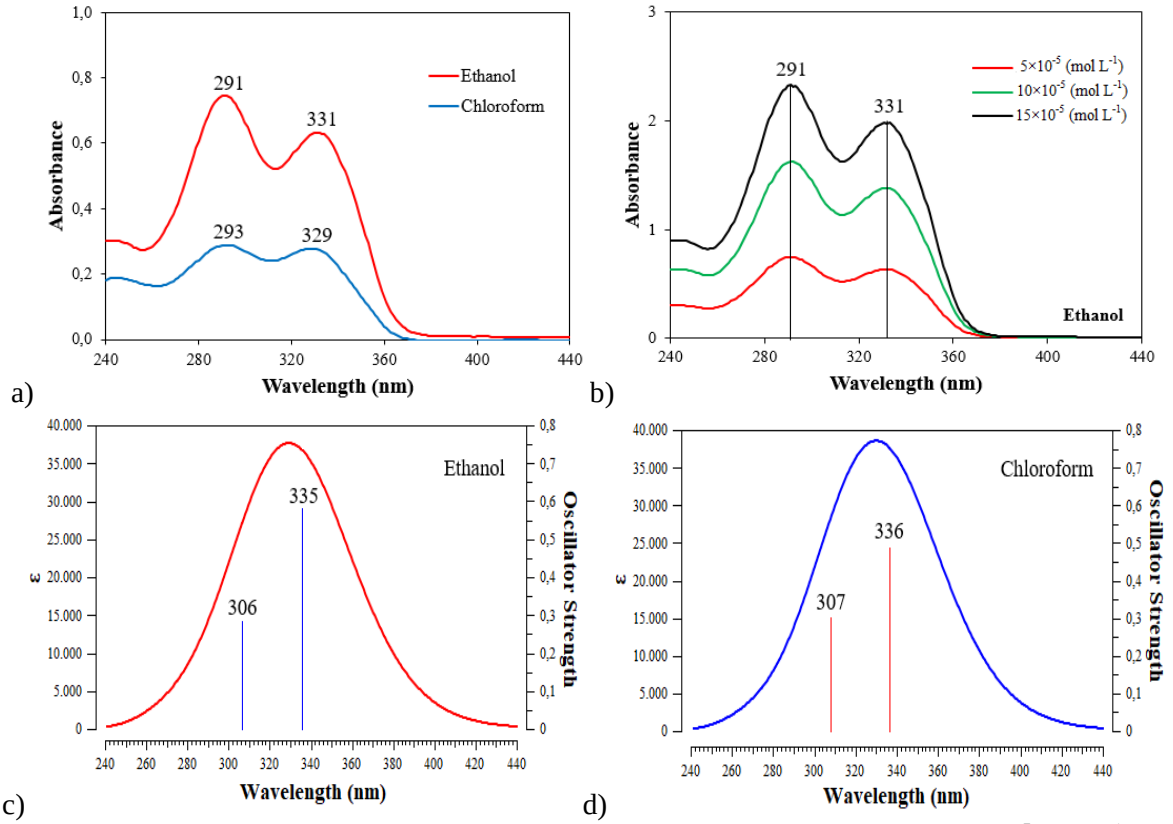


***Figure 7.*** *a) The experimental UV-Vis spectra of HL in ethanol and chloroform ($5\times10^{-5}$ mol $L^{-1}$). b) Absorption spectra of HL in ethanol at three different concentrations. The theoretical UV-Vis spectrum of HL in c) ethanol and d) chloroform*

***Table 3.*** *The electronic absorption spectral values of HL in ethanol and chloroform solvents ($15\times10^{-5}$ mol $L^{-1}$)*

| Solvents | Experimental | | Calculated | | | Assignments |
|---|---|---|---|---|---|---|
| | λ(nm) | E (eV) | λ(nm) | E (eV) | f | |
| Ethanol | 291 | 4.26 | 306 | 4.04 | 0.29 | π-π* |
| | 331 | 3.74 | 335 | 3.69 | 0.77 | n-π* |
| Chloroform | 293 | 4.23 | 307 | 4.02 | 0.30 | π-π* |
| | 333 | 3.72 | 336 | 3.68 | 0.78 | n-π* |

### 3.4. Natural Bond Orbital Analysis

Analysing NBO explains the most important inter and intramolecular bonding interactions, conjugative interactions, hyperconjugative interactions to clarify general structure [33]. Bond type, bond order, hybridization charge, Lewis structures,donor-acceptor interactions and resonance features of molecules can also be explained thanks to that analysis. Meanwhile, the interaction stabilisation energies *E*(2), as well as electron acceptor and donor orbitals, can be summarised with the results obtained from the second-order perturbation theory analysis of the Fock matrix in NBO analysis [30]. Intermolecular hyperconjugative interactions occurring between bonding and antibonding orbitals weaken the character of bonds, thereby causing an increase in electron density in the antibonding orbitals [8]. Intermolecular changes allow load transfer because overlapping orbitals stabilise the molecular system. The important π to π* interactions were observed such as π(C4-C5) → π*(C2-C3) 27.01 kcal/mol, π(C2-C3) → π*(C4-C5) 12.91 kcal/mol, π(C19-C20) → π*(C21-C24) 22.59 kcal/mol, π(C19-C20) → π*(C22-C26) 18.54 kcal/mol, π(C21-C24) → π*(C19-C20) 16.25 kcal/mol, π(C21-C24) → π*(C22-C26) 21.28 kcal/mol, π(C22-C26) → π*(C19-C20) 23.29 kcal/mol, π(C22-C26) → π*(C21-C24) 16.99 kcal/mol. Those results indicate intramolecular charge transfers that provide the structure with stability. The interaction of intramolecular hyperconjugative

stabilization energy of lone pair of electrons from $LP_1$ ($N_9$) atom with antibonding natural of π*(C1-N8) was found 50.38 kcal/mol. This important charge transfer gives stability to the molecule [37]. The other significant hyperconjugative interactions were observed $LP_1$ ($N_9$) → π*(N11-C12) 29.16 kcal/mol and $LP_2$ ($O_{29}$) → π*(C22-C26) 30.67 kcal/mol, respectively. The strongest interactions of HL were computed as π*(C1-N8) → π*(C4-C5), π*(C2-C3) → π*(C4-C5), π*(N11-C12) → π*(C19-C20), π*(C22-C26) → π*(C19-C20) with stabilization energy data of 135.33, 149.06, 104.18, 238.45 kcal/mol, respectively. As a result of NBO analysis of optimized HL molecule, 97.618% the total lewis orbital, 2.382% total non-lewis orbital, 99.965% core orbital, 96.516% valence lewis orbital, 2.219% valence non-lewis orbital, 0.163% rydberg non-lewis orbital were calculated [8].

### 3.5. Frontier Molecular Orbitals (FMOs) Analysis and Global Reactivity

HOMOs and LUMOs have the most important energy levels in any molecule [39,40]. Because the energy difference between LUMOs and HOMOs, as frontier orbitals, plays a important role in the chemical reactivity, stability and electronic transition of molecules, it is largely responsible for determining the spectroscopic and chemical features of the structure [41]. Whereas the LUMO is attributed to electron affinity, the HOMO is attributed to ionisation potential [42]. All orbital energy levels were examined, and four important MOs LUMO+1, LUMO, HOMO and HOMO-1 are shown in Figure 8. In that figure, the red-coloured entities represent positive lobes, whereas the green-coloured entities represent negative ones [37]. According to the DFT/B3LYP calculation, energy values of the band between LUMO–HOMO and LUMO+1–HOMO-1 were 2.5249 eV and 3.6357 eV for the HL molecule. The frontier orbitals thus indicate low chemical reactivity and high kinetic stability [43]. As also shown in Figure 8, HOMOs indwelled in the whole molecule, while LUMOs were mostly concentrated over the 4-methoxyphenyl ring, which highlights the intramolecular charge transfer of the HL [26]. The total dipole moment, another major electronic property in a structure [44], in terms of the $\mu_x$, $\mu_y$ and $\mu_z$ of the HL from the same basis set, were 0.1845, 0.1048 and 0.2230 D, respectively [44]. According to Koopmans theorem, the HOMO level of energy corresponds to the ionization potential (I) while the LUMO level of energy corresponds to the electron affinity (A), ($I = -E_{HOMO}$ and $A = -E_{LUMO}$). The electron affinity and ionization potential of the HL were found as 4.7677 eV and 7.2926 eV, respectively. With this theorem, chemical hardness, chemical softness and electronegativity values of the HL molecule can be calculated [45,46]. The electronegativity (χ) of a compound can be calculated using the equation, $\chi = (I + A)/2$. According to this equation, the electronegativity of the HL was 6.0301 eV. Chemical hardness (η) and chemical softness (S) determine the stability and reactivity of a molecular system. They can be calculated using the equations, $\eta = (I–A)/2$ and $S = 1/2\eta$, respectively. Chemical hardness and softness were found as, $\eta = 1.2624$ eV and $S = 0.3960$ eV. According to these results, it was determined that the HL molecule has high stability [11,47,48].

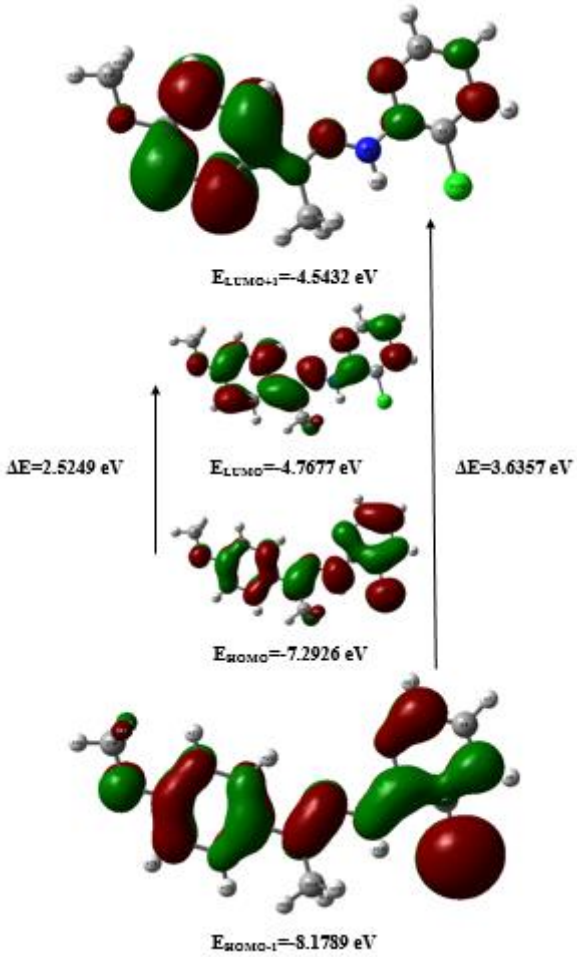


***Figure 8.*** *The frontier molecular orbitals of the HL*

### 3.6. Molecular Electrostatic Potential

The molecular electrostatic potential depends on the charge distribution of the structure [49]. MEP mapping is a highly useful tool for investigating the molecular structure and its physicochemical features and was used in the study to elucidate charge–dipole, quadrupole–dipole and dipole-dipole interactions as well as the electrostatic potential value, molecular shape and molecular size [32]. The mapping process was applied onto the electron density surface and used to visualise charge distributions in the molecules. In MEP mapping, the red-coloured entities represent negative regions and sites for the electrophilic attack, whereas the blue-coloured entities represent the positive regions and sites for the nucleophilic attack. The electrostatic potential values decreased from blue to red. The MEP values of the map lie between -6.461 (i.e. dark red) and 6.461 $e^{-2}$ a.u (i.e. dark blue) for the HL molecule, wherein the red colouring indicates the repulsion and the blue colouring indicates the attraction [34]. In the examined molecule, the negative regions were primarily spread over the hydrazone group of nitrogen atoms and the methoxy group of the oxygen atom. From the obtained results, N9, N11 and 029 atoms demonstrated the strongest repulsion [50]. The MEP surface is illustrated in Figure 9.

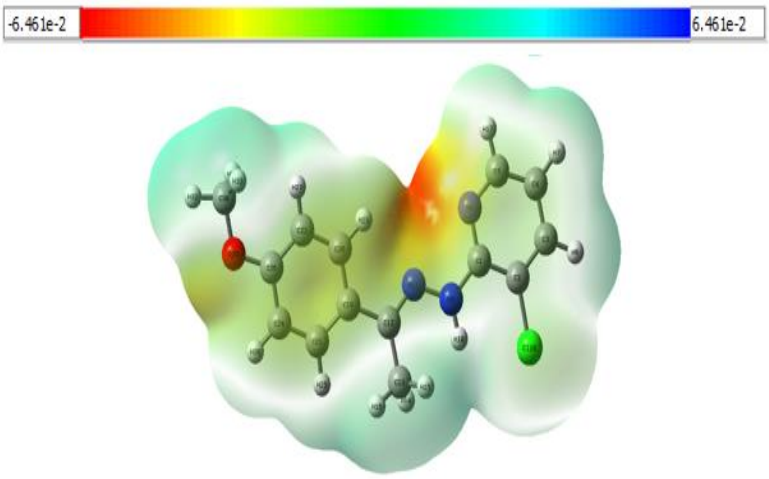


***Figure 9.*** *The molecular electrostatic potential (MEPs) for HL*

## 4. CONCLUSIONS

The synthesised compound was characterised by analytical and spectral data. MEP analysis suggested that the major reactive centres of the pyridine and hydrazone derivatives of the HL molecule were N9, N11 and 029 atoms indicating electrophilic attack and the strongest repulsion. The HOMO–LUMO energy gap was examined at 2.5249 eV, and whereas LUMOs were mostly spread over the 4-methoxyphenyl ring, HOMOs were distributed across the entire HL molecule. Observed UV-Vis of HL molecule and chemical shifts of carbon and hydrogen atoms showed excellent agreement relative to theoretical calculations for the compound. Valuable results were obtained from NBO analysis to clarify the properties and activity of the molecule. The correlation between the recorded and calculated FT-IR frequencies with the scaling factor of the fitting factor ($R^2$) was 0.9993. By studying the HL compound reported herein and its chemical properties, researchers can pinpoint applications for the design of new inorganic materials with improved properties. Another outcome of the study is its potential contribution to in silico and in vivo studies to aid the treatment of various diseases due to the high chemical stability of the HL molecule.

## CONFLICT OF INTEREST

No conflict of interest was declared by the author.

## ACKNOWLEDGMENT

The calculations reported in this manuscript were partially/completely performed at TUBITAK ULAKBIM, Grid Computing Center and High Performance (TRUBA resources). I would like to thank the lecturer Süleyman Çelik for his contribution.

## REFERENCES

[1] Adly, O. M. I., and Emara, A. A. A., "Spectroscopic and biological studies of new binuclear metal complexes of a tridentate ONS hydrazone ligand derived from 4-amino-6-methyl-3-thioxo-3,4-dihydro-1,2,4-triazin-5(2H)-one and 4,6-diacetylresorcinol", Spectrochimica Acta Part A: Molecular and Biomolecular Spectroscopy, 132: 91-101, (2014).

[2] Clark, N. A., Coleman, D., and Maclennan, J. E., "Electrostatics and the electro-optic behaviour of chiral smectics C: ‘block’ polarization screening of applied voltage and ‘V-shaped’ switching", Liquid Crystals, 27: 985–990, (2000).

[3] Da Cunha Areias, M. C., Ávila-Terra, L. H. S., Gaubeur, I., and Suárez-Iha, M. E. V., "A new simultaneous spectrophotometric method for determination of iron(II) and iron(III) in natural waters", Spectroscopy Letters, 34: 289–300, (2001).

[4] Rollas, S., and Küçükgüzel, Ş. G., "Biological activities of hydrazone derivatives", Molecules, 12: 1910–1939, (2007).

[5] Karadeniz, Ş., Ataol, C. Y., Şahin, O., İdil, Ö., and Bati, H., "Synthesis, structural studies and antimicrobial activity of N'-((2Z, 3E)-3-(hydroxyimino)butan-2-ylidene)-2-phenylacetohydrazide and its Co(II), Ni(II) complexes", Journal of Molecular Structure, 1161: 477–485, (2018).

[6] Schlosser, M., and Mongin, F., "Pyridine elaboration through organometallic intermediates: regiochemical control and completeness", Chemical Society Reviews, 36: 1161–1172, (2007).

[7] Mohamed Asath, R., Premkumar, R., Mathavan, T., and Milton Franklin Benial, A., "Structural, spectroscopic and molecular docking studies on 2-amino-3-chloro-5-trifluoromethyl pyridine: A potential bioactive agent", Spectrochimica Acta Part A: Molecular and Biomolecular Spectroscopy, 175: 51–60, (2017).

[8] Uzun, S., Demircioğlu, Z., "Bis[2-(metilamino)troponato]bakır(II) Molekülünün Yapısal ve Elektronik Özelliklerinin Deneysel ve Kuramsal Analizleri", Süleyman Demirel Üniversitesi Fen Edebiyat Fakültesi Fen Dergisi, 15: 9–22, (2020).

[9] Topal, T., Kart, H. H., Tunay Taşlı, P., and Karapınar, E., "Synthesis and structural study on (1E,2E,1′E,2′E)-3,3′-bis[(4-bromophenyl)-3,3′-(4-methy-1,2-phenylene diimine)] acetaldehyde dioxime: A combined experimental and theoretical study", Optics and Spectroscopy, 118: 897–912, (2015).

[10] Malik, M., Wysokiński, R., Zierkiewicz, W., Helios, K., and Michalska, D., "Raman and infrared spectroscopy, DFT calculations, and vibrational assignment of the anticancer agent picoplatin: performance of long-range corrected/hybrid functionals for a platinum(II) complex", The Journal of Physical Chemistry A, 118: 6922-6934, (2014).

[11] Albayati, M. R., Kansız, S., Dege, N., Kaya, S., Marzouki, R., Lgaz, H., Salghi, R., Ali, Ismat., Alghamdi, M. M., Chung, III-Min., "Synthesis, crystal structure, Hirshfeld surface analysis and DFT calculations of 2-[(2,3-dimethylphenyl)amino]-N'-[(E)-thiophen-2-ylmethylidene]benzohydrazide", Journal of Molecular Structure, 1205, 127654, (2020).

[12] Topal, T., "Synthesis, Crystallographic Structure, Hirshfeld Surface Analysis, Drug-likeness Properties and Molecular Docking Studies of New Oxime-pyridine Compounds", Acta Chimica Slovenica, 68: 88-101, (2020).

[13] Frisch, M. J., Trucks, G. W., Schlegel, H. B., Scuseria, G. E., Robb, M. A., Cheeseman, J. R., Scalmani, G., Barone, V., Mennucci, B., Petersson, G. A., Nakatsuji, H., Caricato, M., Li, X., Hratchian, H. P., Izmaylov, A. F., Bloino, J.,Zheng, G., Sonnenberg, J. L., Hada, M., Ehara, M., Toyota, K., Fukuda, R., Hasegawa, J., Ishida, M., Nakajima, T., Honda, Y., Kitao, O., Nakai, H., Vreven, T., Montgomery, J. A., Jr., Peralta, J. E., Ogliaro, F., Bearpark, M., Heyd, J. J., Brothers, E., Kudin, K. N., Staroverov, V. N., Keith, T., Kobayashi, R., Normand, J., Raghavachari, K., Rendell, A., Burant, J. C., Iyengar, S. S., Tomasi, J., Cossi, M., Rega, N., Millam, J. M., Klene, M. , Knox, J. E., Cross, J. B., Bakken, V., Adamo, C., Jaramillo, J., Gomperts, R., Stratmann, R. E., Yazyev, O., Austin, A. J., Cammi, R., Pomelli, C., Ochterski, J. W., Martin, R. L., Morokuma, K., Zakrzewski, V. G., Voth, G. A., Salvador, P., Dannenberg, J. J., Dapprich, S., Daniels, A. D., Farkas, O., Foresman, J. B., Ortiz, J. V., Cioslowski, J. and Fox, D. J. Gaussian, Inc., Gaussian 09, Revision D.01, Wallingford CT, (2013).

[14] Kohn, W. and Sham, L. J., "Self-Consistent Equations Including Exchange and Correlation Effects", Physical Review, 140: A1133-A1138, (1965).

[15] Vladimiroff, T., "A density functional study of s-trinitrobenzene", Journal of Molecular Structure: Theochem, 453: 119–122, (1998).

[16] Panicker, C. Y., Ambujakshan, K. R., Varghese, H. T., Mathew, S., Ganguli, S., Nanda, A. K., and Alsenoy, C. V., "FT-IR, FT-Raman and DFT calculations of 3-{[(4-fluorophenyl)methylene] amino}-2-phenylquinazolin-4(3H)-one", Journal of Raman Spectroscopy, 40: 527–536, (2009).

[17] Jamróz, M. H., "Vibrational energy distribution analysis (VEDA): scopes and limitations", Spectrochimica Acta Part A: Molecular and Biomolecular Spectroscopy,114: 220–230, (2013).

[18] Wolinski, K., Hinton, J. F., and Pulay, P., "Efficient Implementation of the Gauge-Independent Atomic Orbital Method for NMR Chemical Shift Calculations", Journal of the American Chemical Society, 112: 8251–8260, (1990).

[19] Casida, M. E., Casida, K. C., and Salahub, D. R., "Excited-state potential energy curves from time-dependent density-functional theory: A cross section of Formaldehyde's 1A1 manifold", International Journal of Quantum Chemistry, 70: 919–924, (1998).

[20] Glendening, E.D., Reed, A.E., Carpenter, J.E., and Weinhold, F., NBO Version 3.1, (2003).

[21] Frisch, M. J., Trucks, G. W., Schlegel, H. B., Scuseria, G. E., Robb, M. A., Cheeseman, J. R., Scalmani, G., Barone, V., Petersson, G. A., Nakatsuji, H., Li, X., Caricato, M., Marenich, A. V., Bloino, J., Janesko, B. G., Gomperts, R., Mennucci, B., Hratchian, H. P., Ortiz, J. V., Izmaylov, A. F., Sonnenberg, J. L., Williams-Young, D., Ding, F., Lipparini, F., Egidi, F., Goings, J., Peng, B., Petrone, A., Henderson, T., Ranasinghe, D., Zakrzewski, V. G., Gao, J., Rega, N., Zheng, G., Liang, W., Hada, M., Ehara, M., Toyota, K., Fukuda, R., Hasegawa, J., Ishida, M., Nakajima, T., Honda, Y., Kitao, O., Nakai, H., Vreven, T., Throssell, K., Montgomery, J. A., Jr., Peralta, J. E., Ogliaro, F., Bearpark, M. J., Heyd, J. J., Brothers, E. N., Kudin, K. N., Staroverov, V. N., Keith, T. A., Kobayashi, R., Normand, J., Raghavachari, K., Rendell, A. P., Burant, J. C., Iyengar, S. S., Tomasi, J., Cossi, M., Millam, J. M., Klene, M., Adamo, C., Cammi, R., Ochterski, J. W., Martin, R. L., Morokuma, K., Farkas, O., Foresman, J. B., Fox, D. J. Gaussian, Inc., Gaussian 16, Revision A.03, Wallingford CT, (2016).

[22] Dennington, Roy; Keith, Todd A.; Millam, John M. Semichem Inc., GaussView, Version 6, Shawnee Mission, KS, (2016).

[23] Schmidt, M.W., Baldridge, K.K., Boatz, J.A., Elbert, S.T., Gordon, M.S., Jensen, J.H., Koseki, S., Matsunaga, N., Nguyen, K.A., Su, S., Windus, T.L., Dupuis, M., Montgomery Jr, J.A., "General atomic and molecular electronic structure system", Journal of Computational Chemistry, 14: 1347–1363, (1993).

[24] Puviarasan, N., Arjunan, V., and Mohan, S., "FT-IR and FT-Raman studies on 3-aminophthalhydrazide and N-aminophthalimide", Turkish Journal of Chemistry, 26: 323–333, (2002).

[25] Arslan, H., Algül, O., and Onkol, T., "Vibrational spectroscopy investigation using ab initio and density functional theory analysis on the structure of 3-(6-benzoyl-2-oxobenzo[d]oxazol-3(2H)-yl)propanoic acid", Spectrochimica Acta Part A: Molecular and Biomolecular Spectroscopy, 70: 606-614, (2008).

[26] Sas, E. B., Kurt, M., Can, M., Horzum, N., and Atac, A., "Spectroscopic studies on 9H-carbazole-9-(4-phenyl) boronic acid pinacol ester by DFT method", Journal of Molecular Structure, 1118: 124–138, (2016).

[27] Bieńko, D., Malik-Gajewska, M., Walencik, P., Kaj, M., Zierkiewicz, W., Murtaza, G., Ruffer, T., Ahmad, S., "IR and Raman spectroscopic analysis, DFT modeling, and magnetic properties of a nickel(II) complex, [Ni(succ)(H2O)4]n", Journal of Coordination Chemistry, 72: 2215–2232, (2019).

[28] Ramalingam, S., Periandy, S., Mohan, S., "Vibrational spectroscopy (FTIR and FTRaman) investigation using ab initio (HF) and DFT (B3LYP and B3PW91) analysis on the structure of 2-amino pyridine", Spectrochimica Acta Part A: Molecular and Biomolecular Spectroscopy, 77: 73–81, (2010).

[29] Wilmshurst, J., and Bernstein, H., "The vibrational spectra of pyridine, pyridine-4-d, pyridine-2,6-d2, and pyridine-3,5-d2", Canadian Journal of Chemistry, 35: 1183–1194, (2011).

[30] Karabacak, M., Sinha, L., Prasad, O., Asiri, A. M., Cinar, M., Shukla, V.K., "FT-IR, FT-Raman, NMR, UV and quantum chemical studies on monomeric and dimeric conformations of 3,5-dimethyl-4-methoxybenzoic acid", Spectrochim. Acta - Part A Mol. Biomol. Spectrosc., 123: 352–362, (2014).

[31] Colthup, N., "Introduction to infrared and Raman spectroscopy", Elsevier, (2012).

[32] Boopathi, M., Udhayakala, P., Devi, T.S.R., Rajendiran, T. V., "Vibrational spectroscopic (FT-IR , FT-Raman and NMR) and DFT analysis of 2-methoxy-3-(trifluoromethyl) pyridine", Journal of Chemical and Pharmaceutical Research, 7: 1172–1183, (2015).

[33] Agarwal, P., Choudhary, N., Gupta, A., Tandon, P., "Density functional theory studies on the structure, spectra (FT-IR, FT-Raman, and UV) and first order molecular hyperpolarizability of 2-hydroxy-3-methoxy-N-(2-chloro-benzyl)-benzaldehyde-imine: Comparison to experimental data", Vibrational Spectroscopy, 64: 134–147, (2013).

[34] Muthu, S., and Elamurugu Porchelvi, E., "FT-IR, FT-RAMAN, NMR, spectra, normal co-ordinate analysis, NBO, NLO and DFT calculation of N, N-diethyl-4-methylpiperazine-1-carboxamide molecule", Spectrochimica Acta Part A: Molecular and Biomolecular Spectroscopy, 115: 275–286, (2013).

[35] Topal, T., and Karapınar, E., "Synthesis and characterization of new homo and heteronuclear schiff base copper(II) complexesJournal of the Turkish Chemical Society Section A: Chemistry, 5: 785–802, (2018).

[36] Oltean, M., Calborean, A., Mile, G., Vidrighin, M., Iosin, M., Leopold, L., Maniu, D., Leopold, N., Chis, V., "Absorption spectra of PTCDI :", A combined UV–Vis and TD-DFT study", Spectrochimica Acta Part A: Molecular and Biomolecular Spectroscopy, 97: 703–710, (2012).

[37] Madhankumar, S., Muthuraja, P., and Dhandapani, M., "Structural characterization, quantum chemical calculations and Hirshfeld surface analysis of a new third order harmonic organic crystal: 2-Amino-4-methylpyridinium benzilate", Journal of Molecular Structure, 1201: 127151, (2020).

[38] Topal, T., "Synthesis and characterization of zinc(II) complexes with new pyridine-based ligands: crystal structure, Hirshfeld surface analysis, and molecular docking study of lung cancer cell", Journal of Coordination Chemistry, 73: 3203–3222, (2020).

[39] Babur Şaş, E., and Kurt, M., "5-Bromo-1H Benzimidazolun Ft-Raman, Ft-Ir, Nmr ve Dft Hesaplamaları", SAÜ Fen Bilimleri Enstitüsü Dergisi, 21, (2017).

[40] Fukui, K., "Role of frontier orbitals in chemical reactions", Science (80), 218: 747–754, (1982).

[41] Karakurt, T., "3-[(E)-2-(4-fenil-1,3-tiyazol-2-yl)hidrazin-1-yiliden]-indolin-2-on bileşiğinin Tautomer Yapısı Üzerinde Gaz ve Katı Fazında Teorik Hesaplamalar", Afyon Kocatepe Üniversitesi Fen ve Mühendislik Bilimleri Dergisi, 20: 96–102, (2020).

[42] Arivazhagan, M., and Meenakshi, R., "Vibrational spectroscopic studies and DFT calculations of 4-bromo-o-xylene", Spectrochimica Acta Part A: Molecular and Biomolecular Spectroscopy, 91: 419–430, (2012).

[43] Kumar, M., Kariem, M., Sheikh, H.N., Frontera, A., Seth, S.K., Jassal, A.K., "A series of 3D lanthanide coordination polymers decorated with a rigid 3,5-pyridinedicarboxylic acid linker: syntheses, structural diversity, DFT study, Hirshfeld surface analysis, luminescence and magnetic properties", Dalton Transactions, 47: 12318–12336, (2018).

[44] Prabavathi, N., Nilufer, A., and Krishnakumar, V., "FT-IR, FT-Raman and DFT quantum chemical study on the molecular conformation, vibrational and electronic transitions of 1-(m-(trifluoromethyl) phenyl)piperazine", Spectrochimica Acta Part A: Molecular and Biomolecular Spectroscopy, 121: 483–493, (2014).

[45] Islam, S. K. N., "Conceptual Density Functional Theory and its Application in the Chemical Domain", (2018).

[46] Salzner, U., Baer, R., "Koopmans' springs to life", The Journal of Chemical Physics, 131, (2009).

[47] Venkateshan, M., Priya, R.V., Muthu, M., Suresh, J., Kumar, R.R., "Crystal structure, Hirshfeld surface analysis, DFT calculations and molecular docking studies on pyridine derivatives as potential inhibitors of NAMPT", Chemical Data Collections, 23: 100262, (2019).

[48] Guerrab, W., Lgaz, H., Kansız, S., Mague, J., Ansar, M., Marzouki, R., Taoufik, J., Ali, I., Chung, M. Ramli, Y., "Synthesis of a novel phenytoin derivative: Crystal structure, Hirshfeld surface analysis and DFT calculations", Journal of Molecular Structure, 1205: 127630, (2019).

[49] Murray, J. S., and Sen, K., "Molecular electrostatic potentials: concepts and applications", Elsevier, (1996).

[50] Munshi, P., and Guru Row, T. N., "Intra- and intermolecular interactions in small bioactive molecules: cooperative features from experimental and theoretical charge-density analysis", Acta Crystallographica Section B: Structural Science, 62: 612–626, (2006).